Electronic Properties of Single-Walled Carbon Nanotubes

Monica Samec
Office of Science, DOE ERULF
University of Toronto
National Renewable Energy Laboratory
Golden, CO 80401

August 02, 2002

Participant: _____
Signature

Research Advisor: _____
Signature

Table of Contents

Abstract

Electronic Properties of Carbon Nanotubes. MONICA SAMEC (University of Toronto, Toronto, Ontario, Canada M1C 1A5) Randy Ellingson (National Renewable Energy Laboratory, Golden, Colorado 80401)

Single-walled carbon nanotubes (SWNTs) have unique properties that lend themselves to many potential applications. In order for nanotubes to reach their full potential, it is necessary to have comprehensive understanding of their electronic properties. However, acquiring this knowledge presents major challenges. A nanotube's thermal, electrical, and physical properties vary significantly with its diameter and chirality. Since it is not yet possible to synthesize a specific type of nanotubes, scientists must work with samples of many nanotubes with different properties. In this experiment, laser deposition was used to synthesize SWNTs at different pulsewidths. The material was then purified and cast into a 0.1% m.w. film using a Nafion polymer. The UV-Vis NIR spectra of the samples were analyzed, and no significant differences in absorbance regions were found. Long- and short-range dynamical spectra of the 2 μs pulsewidth sample were analyzed. A double exponential curve was fit to the initial ultrafast decay and a single exponential was fit to the slower decay. Based on the dynamics observed in other nanomaterial systems, the faster decays may be attributed to charge carrier cooling and delocalization of charge along the nanotube, and the slower decay may be due to electron-hole recombination. In these measurements, the decay attributed to charge carrier cooling becomes slightly more influential at a higher energy probe pulse.

Category: _____Physical_____

School Author Attends: University of Toronto
DOE National Lab Attended: National Renewable Energy Laboratory
Mentor's Name: Randy Ellingson
   Phone: (303) 384-6464
   E-mail address: Randy_Ellingson@nrel.gov

Presenter's name: Monica Samec
Mailing Address: 60 Reynier Drive
                        Brampton, ON L6Z 1L8
                        Canada
Phone: (905) 840-5838
E-mail address: puckhead13@planet-save.com

Introduction

Single-walled carbon nanotubes (SWNTs) show promise to revolutionize several different areas of technology -- such as hydrogen storage, flat panel displays, and photovoltaics -- because of their unique properties. SWNTs are essentially graphite sheets rolled into a cylinder and capped with pentagonal rings. Their diameters are on the order of nanometers and their length up to 2 mm (Pan *et al*, 1998). Nanotubes can differ in diameter and chirality (the way the graphite is rolled up). These two variables also dictate their electronic, thermal, and structural properties.

Interesting properties of SWNTs include variable bandgap, high current-carrying capacity, hydrogen absorption, and field emission. A study by Wilder *et al.* showed that the bandgap is inversely proportional to the diameter (1998). This opens up the possibility of choosing a nanotube's bandgap, whereas in other materials, the bandgap is an inherent property. Stable current densities of carbon nanotubes are as high as 10^9 A/cm^2 (Collins *et al*, 2000). In contrast, copper wires burn out at around 10^6 A/cm^2. SWNTs have been observed to absorb hydrogen up to 8% by weight (Dillon *et al*, 1997), making them a feasible form of hydrogen storage for fuel cells. Nanotubes have been found to be excellent field emitters, making them suitable for flat panel display applications (Deheer *et al*, 1995).

However, the physical properties of nanotubes are still being discovered and disputed. The difficulty lies within two key factors: One is the fact that nanotubes have a very

broad range of electronic, thermal, and structural properties that change with diameter and chirality. Coupled to that is the problem that diameter and chirality cannot be adequately controlled during synthesis. Yet with the promise that nanotubes hold, it is essential to overcome these obstacles and attempt to gain an accurate understanding of these properties. It is the aim of this project to contribute to this effort.

Materials and Methods

SWNTs were synthesized with a 755 nm alexandrite laser using the laser pulse synthesis technique described by Dillon *et al* (1999). The pulsewidth was varied with runs at 2.0 μs, 1.0 μs, 500 ns, and 200 ns. The carbon targets contained 2.78% m.w. cobalt and 2.77% m.w. nickel, both metal catalysts in SWNT production. Argon was passed through the 1200° C chamber at a rate of 100 sccm, and pressure was held at 620 Torr. The rastor rate was 0.10300 Hz x 0.0400 Hz (approximately a 50% overlap). The power density was, on average, 27 W/cm^2.

The samples were then refluxed with 100 mL of deionized water and 24 mL of 3M HNO_3 at 130° C for 16.5 hours. During this time, the sample dispersed and metals became ionized. The metal ions were filtered out using 0.2 μm alumina filter and deionized water. The sample and filter were dried in a 50° C oven for 30 minutes, making it possible to separate them from each other. The sample was then baked in a 550° C furnace for 30 minutes to remove the carbon matrix via oxidation. For purposes of optical

characterization, the SWNTs were cast into 0.1% m.w. films in nafion perfluorinated ion-exchange resin purchased from Aldrich.

In order to determine the metal content, ~1 mg of the purified sample was accurately weighed and enclosed in platinum foil. It was then heated at 1100°C for one hour. During this time, all carbon present underwent combustion, and all metals were completely oxidized. It is assumed that cobalt and nickel are the only metals present and that they occur in a 1:1 ratio[1]. Thermodynamic phase diagrams indicate the oxidation state of nickel to be NiO under these conditions. There are two oxidation states possible for nickel, and they are dependent on the cooling conditions. Equations (1) and (2) assume the oxidation state of cobalt to be CoO and $CoO_{1.33}$, respectively. From the weight measurement after oxidation, m_{final}, the number of moles of the original metal, x, can be calculated using the molecular weights of the metal oxides, M.

$$m_{final} = x*(M_{NiO}) + x*(M_{CoO}) \qquad (1.)$$

$$m_{final} = x*(M_{NiO}) + x*(M_{CoO1.33}) \qquad (2.)$$

From x, the mass of nickel and cobalt in the original sample can be calculated and the metal content (wt/wt %) can be found using (3):

$$Metal\ Content = (x*M_{Ni} + x*M_{Co})*100/\ m_{initial} \qquad (3.)$$

---

[1] This assumption should be valid as the target used in synthesis contains Ni and Co in a 1:1 ratio.

Linear absorption measurements were carried out using a Cary 500 double beam spectrometer at a spectral resolution of 1 nm.

Transient absorption measurements were taken with a Clark-MXR CPA-2001 regeneratively-amplified Ti:sapphire laser operating at 989 Hz. The 775 nm output pulses pump an optical parametric amplifier. β-BaBO4 (BBO) was used to double the frequency of a fraction of the 775 nm beam. By focusing a small portion of the Ti:sapphire output on a 2 mm sapphire window, white light probe pulses ranging from 440-950 nm were generated. Probe pulses can be delayed up to 1300 ps relative to the pump. The pump and probe pulsewidths are 200 and 125 fs, respectively.

Results

Synthesis generated an average total yield of 104.9 mg per run at an average rate of 23.9 mg/hr. Metal content of the purified samples can be found in Table 1.

UV-Vis NIR spectra were taken of each of the samples and a nafion blank in reference to air. Results can be found in Figure 1. Due to technical difficulties, the Cary 500 spectrophotometer did not record absorbance in the 587-647 nm range for all samples.

Dynamics spectra were taken for the sample synthesized with a 2.0 μs pulsewidth using transient absorption spectroscopy. One long-range dynamical measurement was taken where the delay was varied from 0.5 to 1300 ps, and the sample was pumped at 450 nm

and probed at 650 nm. The sample experienced fast decay followed by a slower one. The faster decay was fitted to a double exponential function, indicating two separate but simultaneous decay processes. The function was fit from 0.116 ps to 10.2 ps , and gave time constants 140 fs and 960 fs occurring at a ratio of 23:1. The slower decay was fit to a single exponential function from 10.2 ps to 1300 ps, and had a decay time of 120 ps. This data is represented in Figure 2.

Two further dynamics spectra were taken from –0.5 to 10 ps delay. One of these, Figure 3, was also pumped at 450 nm, but probed at 530 nm. A double exponential curve was fitted from 0.140 ps to 9.7 ps and the time constants were calculated to be 130 fs and 940 fs in a 24:1 ratio. Figure 4 shows the spectrum of the sample being pumped at 550 nm and probed and 640 nm. The time constants were calculated to be 150 fs and 990 fs in a 12:1 ratio.

Discussion and Conclusions

Overall, the UV-Vis NIR spectra of the four samples (Figure 1) show absorbance in all of the same regions. The nafion blank shows very little absorbance except in the 1914 nm region. In this region, nafion contributes to, but does not account for all of, the absorbance from the nanotube/nafion films. It is possible that nafion might react with the nanotubes to enhance absorption in this area. Absorbance in the 1789 nm region seems to be from the nanotubes themselves. According to the Kataura plot (Saito, 2000), nanotube absorbance at this energy can only be attributable to metallic nanotubes.

The two samples with the shorter pulsewidths, 200 ns and 500 ns, show distinctly less absorbance than the 1.0 and 2.0 μs pulsewidths. It is possible that the high energy intensity attributed to such short pulsewidths could produce less absorbent nanotubes.

However, due to the similar absorbance spectra for all the samples, no structural differences can be derived from the UV-Vis NIR spectrum.

In all three dynamics spectra from transient absorption spectroscopy measurements, we see two very quick decays on the order of 100 and 900 fs. In each case, these decays are in all probability due to the same events. The attribution of these time constants to a physical process is challenging. However, based on the dynamics observed in other nanomaterial systems, we propose that the fastest decay may correspond to charge carrier cooling, and the 900 fs decay may represent the delocalization of charge along the nanotube. We attribute the slower decay of 120 ps, seen in Figure 2a, to electron-hole recombination.

In comparing Figures 2 and 3, we see that for the same pump wavelength of 450 nm, the higher energy probe wavelength of 530 nm resulted in quicker decay times and a slightly increased influence of the faster decay. In Figure 4, we see that for a less energetic pump pulse, both decays become longer and that the influence of the 990 fs decay increases dramatically.

The main conclusions from this stage of the project are that the UV-Vis NIR spectra shows that the four samples have no significant structural differences although nanotubes synthesized with a shorter pulsewidth tend to show less absorption, potentially because of nanotube degradation due to high energy intensity. Transient absorption data indicates that the two fast decays, potentially due to charge carrier cooling and charge delocalization along the nanotube, become slower with a less energetic pump pulse. Also the decay attributed to charge carrier cooling becomes slightly more influential at a higher energy probe pulse.

There is much more work to be done on this project. Further transient absorption measurements, as well as Raman and photoluminescence measurements, are needed to more fully analyze all four samples. Data from these samples can also be compared to samples produced from different methods to compare different structures.

Acknowledgements

Figures and Table

Table 1: Synthesis and Purification Results

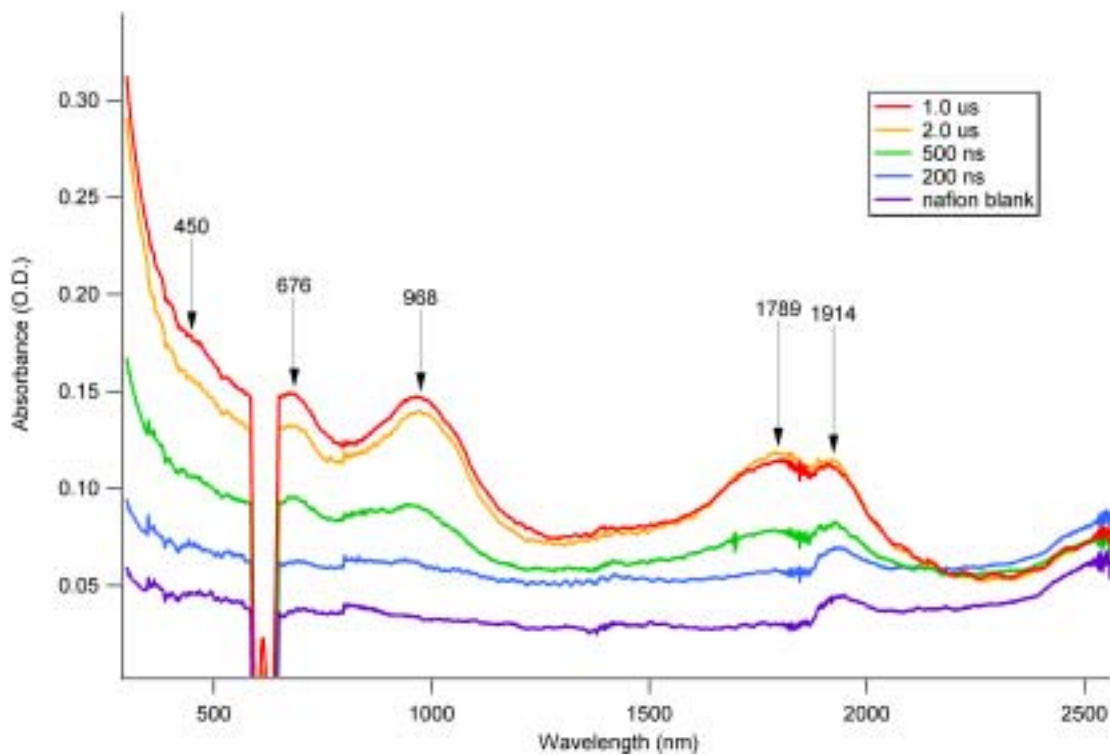| Sample	Pulsewidth	Film thickness	Metal content (wt/wt %)
LP020710	1.0 μs	30 μm	3.77
LP020715	500 ns	34 μm	4.32
LP020717	2.0 μs	34 μm	3.27
LP020718	200 ns	35 μm	1.75

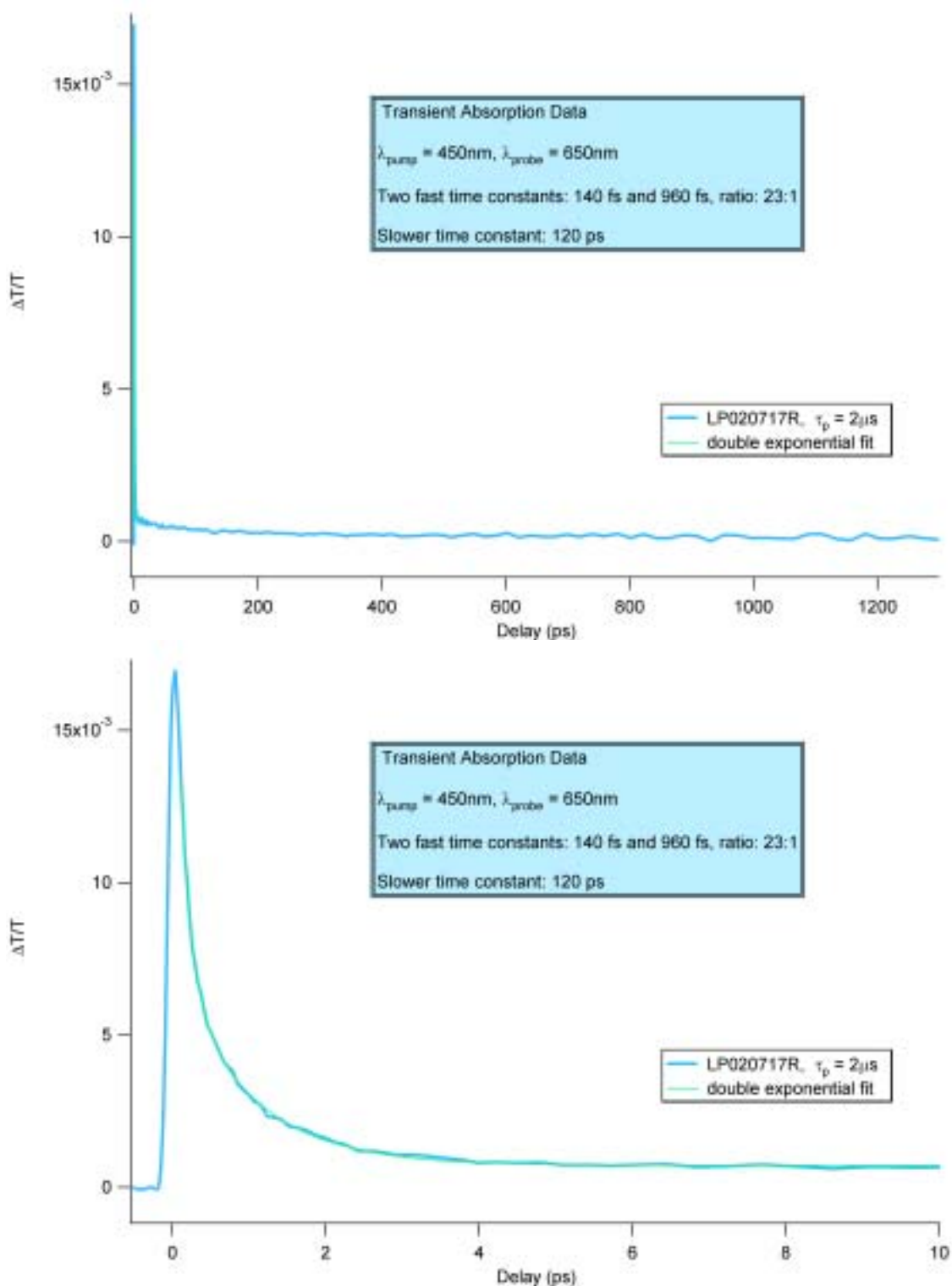**Figure 1: UV-Vis NIR Spectra of SWNTs of Varied Pulsewidth in Nafion vs. Air**

Figure 2: Transient Absorption dynamics spectra of sample LP020717R (generated with a 2.0 µs pulsewidth) pumped at 450 nm and probed at 650 nm a) from –0.5 to 1300 ps delay and b) from –0.5 to 10 ps delay.
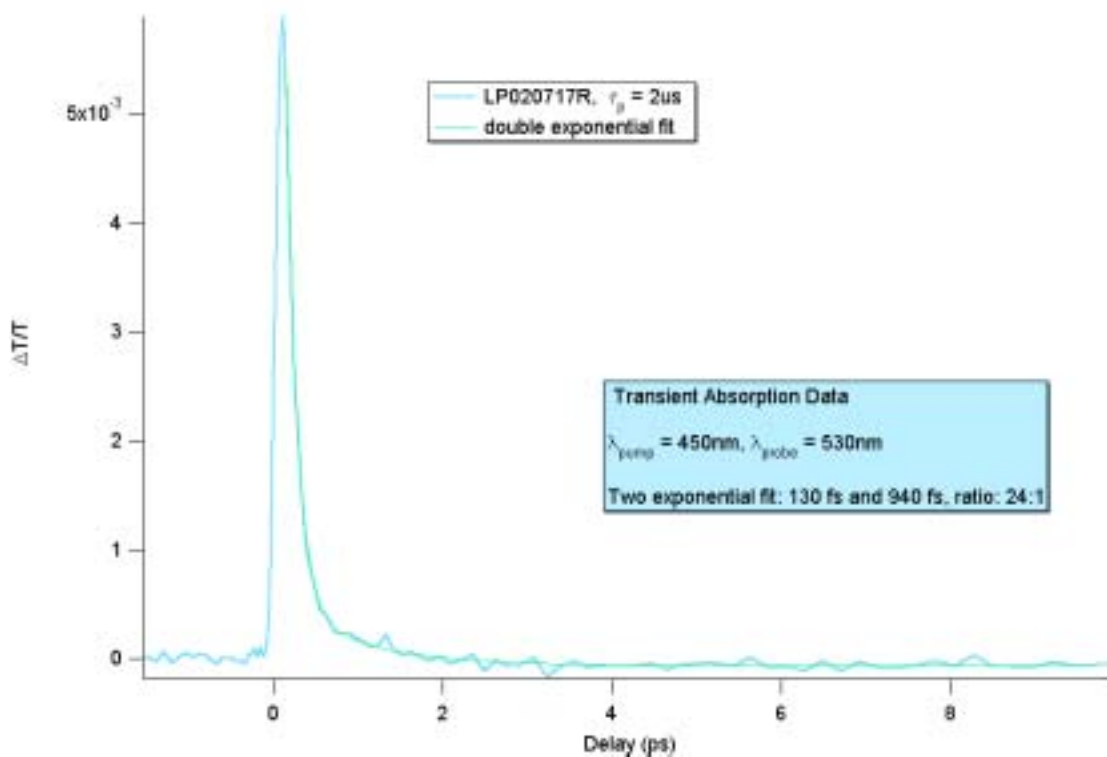
Figure 3: Transient Absorption dynamics spectra of sample LP020717R (generated with a 2.0 μs pulsewidth) pumped at 450 nm and probed at 530 nm from −0.5 to 10 ps delay.
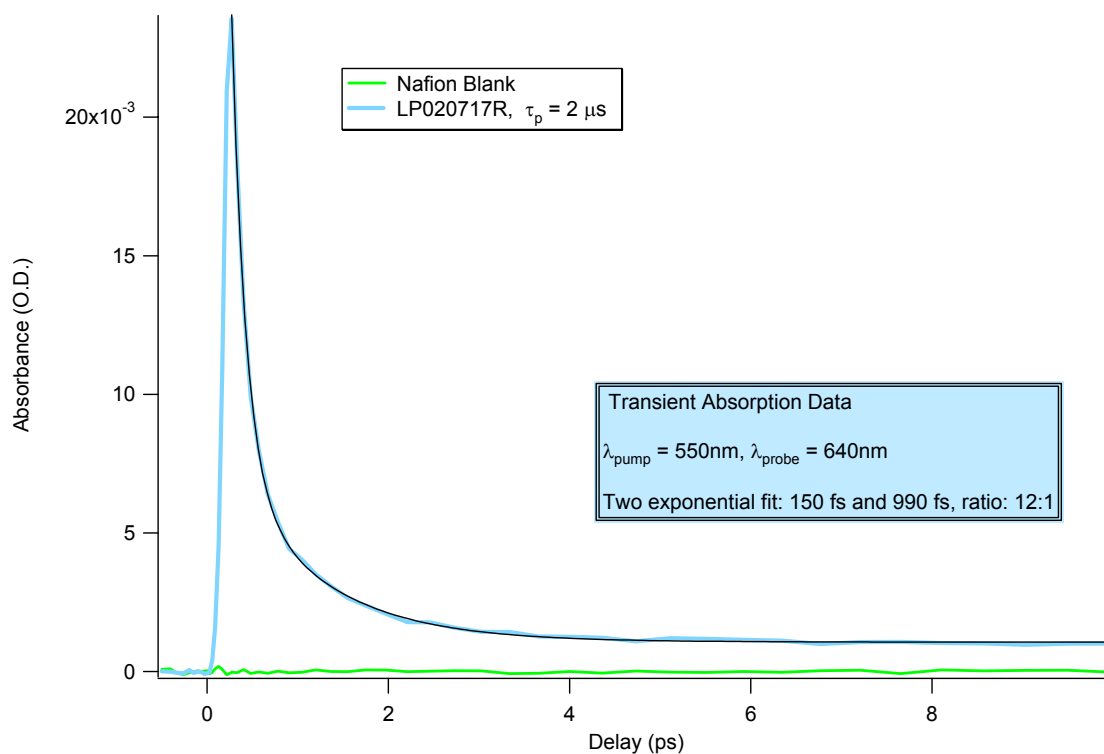

Figure 4: Transient Absorption dynamics spectra of sample LP020717R (generated with a 2.0 μs pulsewidth) pumped at 550 nm and probed at 640 nm from −0.5 to 10 ps delay.

References

Collins, P.G., Avouris, P. (2000, December) "Nanotubes for Electronics" <u>Scientific American</u>, pp 62-69.

Deheer, W.A., Chatelain, A., Ugarte, D. (1995, November 17). "A Carbon Nanotube Field- Emission Electron Source" <u>Nature</u>, pp 1179-1180.

Dillon, A.C., Gennett, T., Jones, K.M., Alleman, J.L., Parilla, P.A., Heben, M.J. (1999, November 10) "A Simple and Complete Purification of Single-Walled Carbon Nanotube Materials" <u>Advanced Materials</u>, pp1354-1358.

Dillon A.C., Jones K.M., Bekkedahl T.A., Kiang C.H., Bethune D.S., Heben M.J. (1997, March 27) "Storage of hydrogen in single-walled carbon nanotubes" <u>Nature</u>, pp 377-379

Pan, Z.W., Xie S.S., Chang B.H., Wang C.Y., Lu L., Liu W., Zhou, W.Y., Li, W.Z., Qian, L.X. (1998, August 13) "Very Long Carbon Nanotubes" <u>Nature</u>, pp 631 – 632.

Saito R., Dresselhaus G., Dresselhaus M.S. (2000, January 15) "Trigonal Warping Effect of Carbon Nanotubes" <u>Physical Review B</u>, pp 2981-2990

Wilder, Jeroen W. G., Venema, Liesbeth C., Rinzler, Andrew G., Smalley, Richard E., Dekker, Cees. (1998, January 1) "Electronic Structure of Atomically Resolved Carbon Nanotubes" <u>Nature</u>, pp. 59-62.